Jestr

Journal of Engineering Science and Technology Review 17 (1) (2024) 131 - 139

Research Article

JOURNAL OF
**Engineering Science and Technology Review**

www.jestr.org

# Study on Crack Propagation Characteristics of Foam Concrete–Soil Composite with Different Height Ratios under Dynamic and Static Loading Conditions

**Xian Liu[1,2], Feiyue Liu[1,2,*], Zhiqiang Yin[2,3], Pinghua Zhu[4] and Minggang Wang[4]**

[1]*Coal Mine Safety Mining Equipment Innovation Center of Anhui Province, Anhui University of Science and Technology, Huainan, 232001, China*
[2]*School of Mining Engineering, Anhui University of Science and Technology, Huainan 232001, China*
[3]*Key Laboratory of Safety and High-Efficiency Coal Mining of Ministy of Education, Anhui University of Science and Technology, Huainan 232001, China*
[4]*China Railway Fourth Bureau Group Fifth Engineering Co., Ltd, Jiujiang 332000, China*

Received 3 December 2023; Accepted 22 February 2024

***Abstract***

Foam concrete is often used for the backfill of subgrade in road engineering to decrease differential settlement, thus forming the foam concrete–soil composite that bears the road dynamic and static loads together. Crack propagation of foam concrete–soil with different backfill depths is a critical factor that influences subgrade stability, and a reasonable study on crack propagation is of great importance to road traffic safety. To explore the crack propagation characteristics of foam concrete–soil subgrade with different backfill depths in traffic dynamic and static loading environments, foam concrete–soil samples with varying ratios of height of 3:1, 1:1, and 1:3 were designed to perform compression and vibration tests. Crack propagation processes of foam concrete–soil samples with different height ratios under dynamic and static loading conditions were also investigated. Crack damage modes and crack propagation scales were analyzed by combining the Gaussian mixture model and the acoustic emission b value. Results demonstrate that, the porous structures inside the foam concrete interlock mutually upon compression; thus, the thicker the foam concrete layer is, the greater the bearing capacity of the combination after failure. The bearing capacity after the fracture failure of the composite increases from 0.278 MPa to 2.036 MPa. In the composite, cracks initiate from soil mass under dynamic and static loading conditions and spread upward gradually, breaking through the interface and forming through cracks of the foam concrete–soil composite. With the increase in thickness of the foam concrete layer, the proportion of shear cracks under vibration increases from 19.1% to 75.4%, and the fracture mode changes from the tensile fracture-dominated mode to the shear failure-dominated mode. Compared with uniaxial compression, the acoustic emission b value of the composite increases substantially due to the intense energy storage behavior before the development of macroscopic fracture under vibration loads. The proposed novel method provides remarkable evidence for analyzing the crack propagation characteristics of foam concrete–soil subgrade with different backfill depths and evaluating and enhancing its stability.

*Keywords:* Foam concrete–soil composite, Vibration test, Gaussian mixture model, Crack propagation, Crack damage mode

## 1. Introduction

Recent years have witnessed the rapid development of highway and urban road construction and traffic tools in China, and more attention has been paid to subgrade construction projects and the differential settlement between structures and foundation soils in road construction projects. As a building material, foam concrete has unique, excellent properties, such as small unit weight, high fluidity, and good sound insulation [1]. According to the principle of stress compensation, foam concrete can effectively decrease the foundation's additional stress and post construction settlement. In road construction, foam concrete is often used for the backfill of subgrade, thus forming the foam concrete–soil composite structure that bears stress together. Situated in complicated environments, the foam concrete–soil composite reaches not only various static loads like the gravity of structures, vehicles, and long-term debris on roads but also dynamic disturbance of vibrations produced during the operation of vehicles due to uneven roads and vibration behaviors of cars. Additionally, different backfill depths of foam concrete can be chosen according to other working conditions in practical fields [2]. Hence, viewing the foam concrete backfilled subgrade as a composite structure composed of foam concretes and soils with different thicknesses is practical and reasonable. Composites with varying height ratios have different mechanical properties [3]. Accordingly, the mechanical responses upon load disturbance also differ significantly. Hence, studying the crack propagation characteristics of foam concrete–soil composite with varying height ratios under dynamic and static loading conditions has practical importance.

The foam concrete backfilled subgrade may develop different degrees of damage and cracks in response to long-term load disturbance, thus influencing road traffic safety. Previous studies on foam concrete used as building materials emphasize its properties [4]. However, such safety problems are not only determined by the mechanical properties of foam concrete but also related to the overall structure and the performance height of foam concrete–soil composite. The mechanical responses of foam concrete–soil composite differ from those of single foam concrete material. Consequently, a deep study on mechanical behaviors and crack propagation of foam concrete–soil composite under load disturbance has essential relevance in evaluating the

*E-mail address: liufeiyue@aust.edu.cn
ISSN: 1791-2377 
doi:10.25103/jestr.171.17

safety of foam concrete backfilled subgrade. Concerning studies on load disturbance, many scholars conducted uniaxial compression tests [5], triaxial tests [6], four-point bending tests [7], vibration table tests [8], and other tests. The above studies focused on single static tests or dynamic tests. Nevertheless, foam concrete–soil composites with different backfill depths bear disturbances of several dynamic and static loads in the practical traffic environment. Combining static and dynamic tests, the microscopic failure mechanism and crack propagation characteristics of foam concrete–soil composite with different height ratios shall be further studied and discussed.

On this basis, three foam concrete–soil samples with different height ratios were designed to simulate foam concrete subgrades with varying depths of backfill. The prepared composite samples' crack propagation processes, damage modes, and crack propagation scales under static and dynamic loading conditions were analyzed through uniaxial compression and vibration table tests. The study results provide an experimental basis for further research on foam concrete backfilled subgrades with different backfill depths.

## 2. State of the art

Due to its characteristics, foam concrete has been extensively applied to practical fields, and relevant studies on foam concrete backfill have been carried out by many scholars. Huang et al. [9] implemented the long-term monitoring of performances of the transition section of the foam concrete backfilled railway subgrade and found the maximum relevant error of the base settlement along the longitude direction was only 3.76 mm. This result proved foam concrete was conducive to controlling the differential settlement between the subgrade and the framework culvert. Through the dynamic triaxial test and the construction of the numerical model of filling a widened embankment, Shi et al. [10] found the embankment surface settlement, soil pressure on the foundation surface, and horizontal deformation of the foundation decreased substantially by using the light foam concrete as the filling material of the widened embankment. Based on the results of the above study, foam concrete has apparent advantages over other filling materials like filling soils. However, foam concrete often forms composite structures with various materials in practical fields to bear external environmental loads together. Hence, studying the foam concrete composite structure is particularly important. Yang et al. [11] prepared the foam ceramics–foam concrete composite wall using the direct casting method for compression and tensile tests. They also analyzed and discussed the failure mechanism of the composite structure. They found the foam ceramic plate with a density of 410 kg/m$^3$ applicable to composite wall panels. Zhou et al. [12] proposed a composite structure composed of a top layer of basalt fiber-constrained waste brick particles (BFCBP) and a bottom layer of foam concrete. They carried out a quasi-static compression test of the structure. They found the aspect ratio of BFCBP and foam concrete substantially influenced the composite structure's failure mode and energy absorption. Portal et al. [13] conducted quasi-static and cyclic quasi-static four-point bending tests of the carbon fiber-enhanced concrete–foam concrete (TRC-FC) composite structure. They found the TRC-FC composite structure has good bearing capacity, partial recombination effect, and excellent ductility. To sum up, the foam concrete composite structure has good properties and broad application prospects. However, studies on foam concrete composite structures always focus on a practical component, and the foam concrete backfilled subgrade is large in the project field. In addition, studying the overall subgrade consumes considerable workforce and material resources, and these experiments are also of long circles. Hence, foam concrete–soil samples need to be made similar to foam concrete backfilled subgrade according to the similarity principle and their crack propagation characteristics analyzed.

The influences of loading mode on the mechanical performances of foam concrete cannot be ignored in the experimental simulation study of crack propagation of foam concrete backfilled subgrade under dynamic and static loading conditions. Flores-Johnson et al. [14] studied the mechanical performances of a U-shaped wall formed by fiber-enhanced foam concrete under dynamic cyclic loading conditions through a vibration table test and numerical simulation. They found the U-shaped wall had good antiseismic performances. Murad et al. [15] conducted compression tests of the modified foam concrete-filled hollow sections (FCFHS-FA) with different thicknesses. They found the FCFHS-FA samples developed buckling failure, and local buckling occurred at the top and bottom. Valaskova et al. [16] conducted a vertical vibration test and numerical simulation study of foam concrete samples. They analyzed the dynamic effect of the pavement structure with the foam concrete layer. They found foam concrete had good damping potentials under low-frequency vibrations. Therefore, compression and vibration tests are essential methods to study the mechanical response characteristics of materials under dynamic and static loads. Nevertheless, these studies are single static or dynamic tests. The contrastive analysis combining dynamic and static loading conditions better conforms to the practical field. In addition, appropriate monitoring means have to be chosen to acquire the crack propagation characteristics of foam concrete–soil composites reasonably under dynamic and static loading conditions. Acoustic emission, a non-destructive monitoring means, can accurately detect damages and crack propagation of materials under loading conditions [17]. The method of combining acoustic emission with dynamic and static loading tests and the damage failure characteristics of foam concrete–soil subgrade with different backfill depths under traffic environmental loads still have to be further studied.

To address the lack of existing related studies, three foam concrete–soil samples with different height ratios of 1:3, 1:1, and 3:1 are designed according to the similarity ratio to simulate foam concrete subgrade with varying depths of backfill. The static loading pressure of the subgrade is simulated by uniaxial compression, the vibration environment of the subgrade under moving loads of vehicles is replicated by using a vibration table, and the deformation failure inside the composite is monitored by combining with acoustic emission. The crack propagation characteristics of foam concrete–soil composites with different height ratios under dynamic and static loading conditions are analyzed comprehensively. The results of this study provide test data for further studies on the stability evaluation and enhancement of foam concrete subgrade with different backfill depths.

The remainder of this study is organized as follows. Section 3 briefly describes the similarity test as well as the test apparatus and methodology. Section 4 first analyzes the uniaxial compression stress–strain characteristics of foam

concrete–soil composites with different height ratios, discusses the crack propagations of foam concrete–soil composites under uniaxial compression and vibration effects, studies the crack damage modes of composites under dynamic and static loading conditions through Gaussian mixture clustering, and finally examines the crack propagation scales of composites under dynamic and static loading conditions by combining energy release and b values. Section 5 summarizes the results of this study and provides relevant conclusions.

## 3. Methodology

### 3.1 Similarity ratio and test materials

With comprehensive considerations to test requirements on the dimensional limit of molds and dimensional limit of vibration tables, the similarity ratios of geometric size ( $L$ ), density ( $\rho$ ), and acceleration speed ( $a$ ) in the test model are determined to $C_L = 40$, $C_\rho = 1$, and $C_a = 1$, respectively.

Complicated stresses exist among subgrades. Making all parameters similar is difficult. Hence, the similarity ratios of the model are approximate, and the models are prepared with raw materials. Foam concrete is prepared with foaming agent, cement, and water using the prefabricated foam method as follows: Foam agent is diluted at a ratio of 60 and foamed. Cement and water are mixed according to the mixing ratio and stirred into the cement paste. Later, an appropriate amount of foam is collected according to the mixing ratio and poured into the cement paste for secondary stirring into foam concrete. The mixing ratios of foam concrete are listed in Table 1.

**Table 1.** Mixing ratio of foam concrete

| Water cement ratio | Cement (kg/m$^3$) | Water (kg/m$^3$) | Foam (kg/m$^3$) |
|---|---|---|---|
| 0.6 | 350 | 210 | 33.85 |

**Table 2.** Physical and mechanical parameters of soil

| Unit weight (kN/m$^3$) | Poisson ratio | Cohesion (kPa) | Internal friction angle (°) | Modulus of elasticity (MPa) |
|---|---|---|---|---|
| 18.7 | 0.33 | 10.3 | 10.3 | 10 |

The material similarity ratio must meet the dynamic and static loading test requirements. Besides, it shall guarantee the dynamic stress–dynamic strain relationship of the subgrade soil and model soil meets the similarity ratio throughout the test. According to the similarity relation and test requirements, clay, river sand, and water (mass mixing ratio of 1:1.5:0.35) are used to simulate subgrade soil (silty clay) [18]. The main physical and mechanical parameters of soil are shown in Table 2.

In this test, the subgrade's length, width, and height are 12, 4, and 2 m, respectively. The backfill depths of foam concrete are 1.5, 1, and 0.5 m. According to similarity conversion, the overall size of foam concrete–soil samples in the dynamic vibration table test is 300 mm×100 mm×50 mm. Specifically, the heights of foam concrete are 37.5, 25, and 12.5 mm, and the corresponding height ratios of the foam concrete–soil composite are 3:1, 1:1, and 1:3, respectively. These three composite samples are numbered Z1, Z2, and Z3. In the uniaxial compression test, the cylinder standard size (Φ50 mm×100 mm) is chosen as the sample size with comprehensive considerations to test the requirements. The corresponding heights of foam concrete are 75, 50, and 25 mm, and the corresponding height ratios of the foam concrete–soil are 3:1, 1:1, and 1:3, denoted as A1, A2, and A3, respectively. The samples are prepared as follows: (1) Similar materials are mixed uniformly according to the designed mixing ratio, and the soil mass of the composite is calculated according to the required degree of compaction (0.95). (2) The corresponding mass of soils is weighed and compacted layer by layer. (3) Foam concrete is poured in the upper layer, applied static for 1 d, and demolded. The final foam concrete–soil samples with different height ratios are shown in Fig. 1.

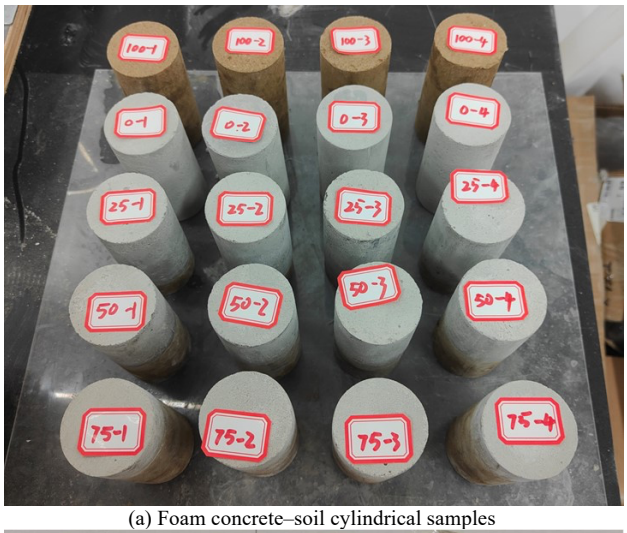


(a) Foam concrete–soil cylindrical samples

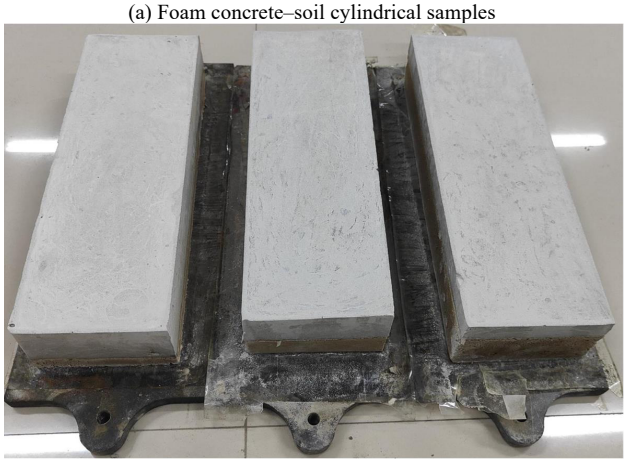

(b) Foam concrete–soil cuboid samples

**Fig. 1.** Foam concrete–soil samples with different height ratios

### 3.2 Test apparatus and test process

A uniaxial compression test is carried out using an RMT-150B rock mechanic testing machine, in which stress loading mode is applied, and the loading rate is 0.1 kN/s. The acoustic emission monitoring system uses the DS2 all-information acoustic emission integrated machine. The synchronous monitoring of composites and stress loading are performed based on acoustic emission. The acoustic emission threshold is 26 dB, and the gain of the preamplifier is 40 dB. Two acoustic emission probes are set on two sides of the middle section of the cylindrical samples. The uniaxial compression system is shown in Fig. 2.

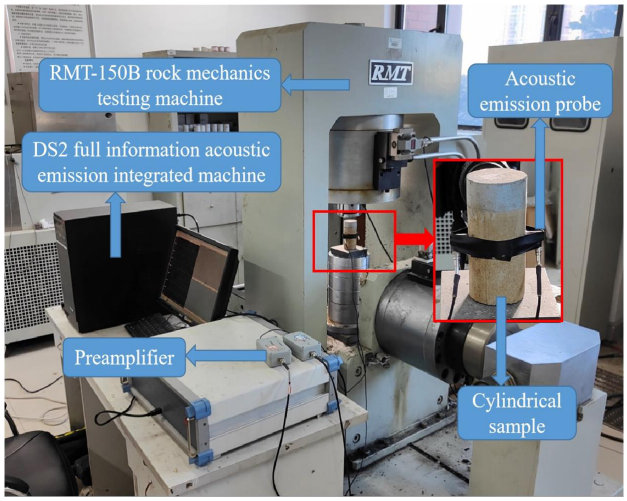


**Fig. 2.** Uniaxial compression system

A vibration test is designed to simulate the vibration environment of the foam concrete–soil subgrade under cyclic loads of pavement and vehicles. Real-time monitoring is performed by acoustic emission. The vibration system is shown in Fig. 3. The GDSF-60XT vibration table is used. Because vibration produced by vehicle loads concentrates in the frequency band of 10–40 Hz [19], the frequency, amplitude, and acceleration are set to 20 Hz, 2.52 mm, and 2.01 g, respectively, considering comprehensive test requirements. The DS2 all-information acoustic emission machine is used. Four acoustic emission probes are set. The distribution of acoustic emission probes is shown in Fig. 4. The acoustic emission threshold, gain of the preamplifier, and sampling rate are 100 dB, 40 dB, and 3 MHz, respectively.

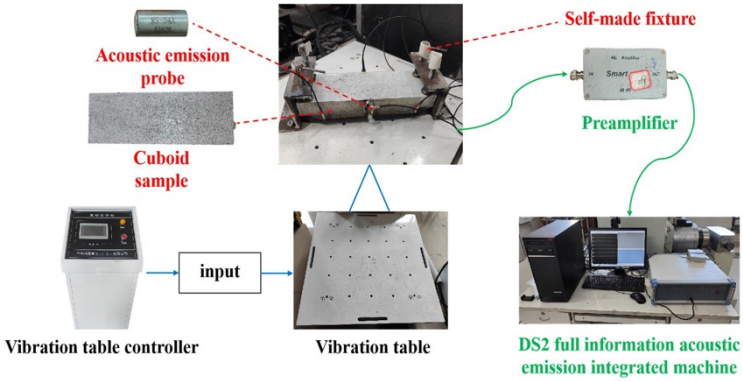


**Fig. 3.** Vibration system

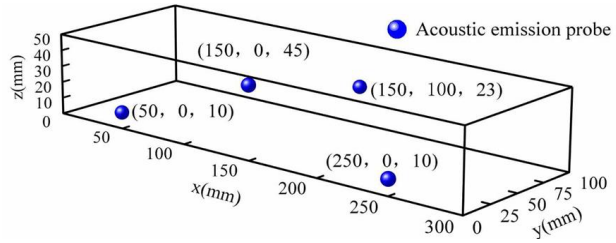


**Fig. 4.** Distribution of acoustic emission probes

## 4. Result Analysis and Discussion

### 4.1 Crack propagation characteristics of composites under uniaxial compression

Based on the uniaxial compression test results in Section 3.2, the stress–strain curves of foam concrete–soil composites with different height ratios are plotted, as shown in Fig. 5. Fig. 5 shows the uniaxial compressive strengths of A1, A2, and A3 are 2.972, 1.783, and 1.131 MPa, respectively. With the decrease in thickness of the foam concrete layer, the compressive strengths of composites present a descending trend because internal cavities of foam concrete are bonded more tightly than those in soils. As a result, samples with a higher foam concrete thickness must accumulate more elastic energy to break cohesion in cell bodies and damage cavities, resulting in higher compressive strength. Moreover, the stress–strain curve shows the uniaxial compressive responses of three foam concrete–soil composites with different height ratios exhibit evident stages, namely, the compaction stage, elastic stage, plastic stage, and post-peak failure stage. Combining different stages of the stress–strain curves and crack evolutionary morphologies of composite surfaces, the crack propagation characteristics of composites could be better analyzed. The crack evolutions on surfaces of A1, A2, and A3 are shown in Fig. 6.

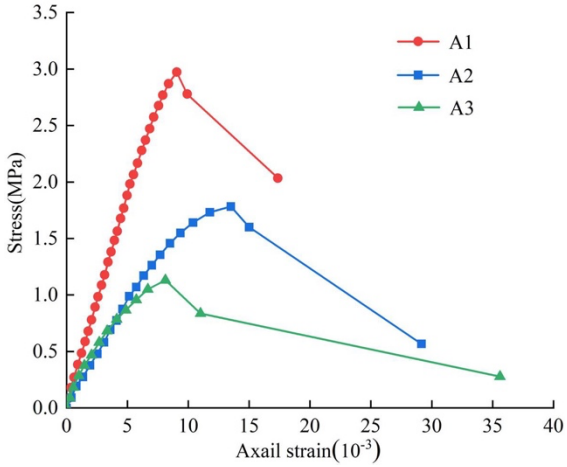


**Fig. 5.** Stress-strain curves of foam concrete–soil composites with different height ratios

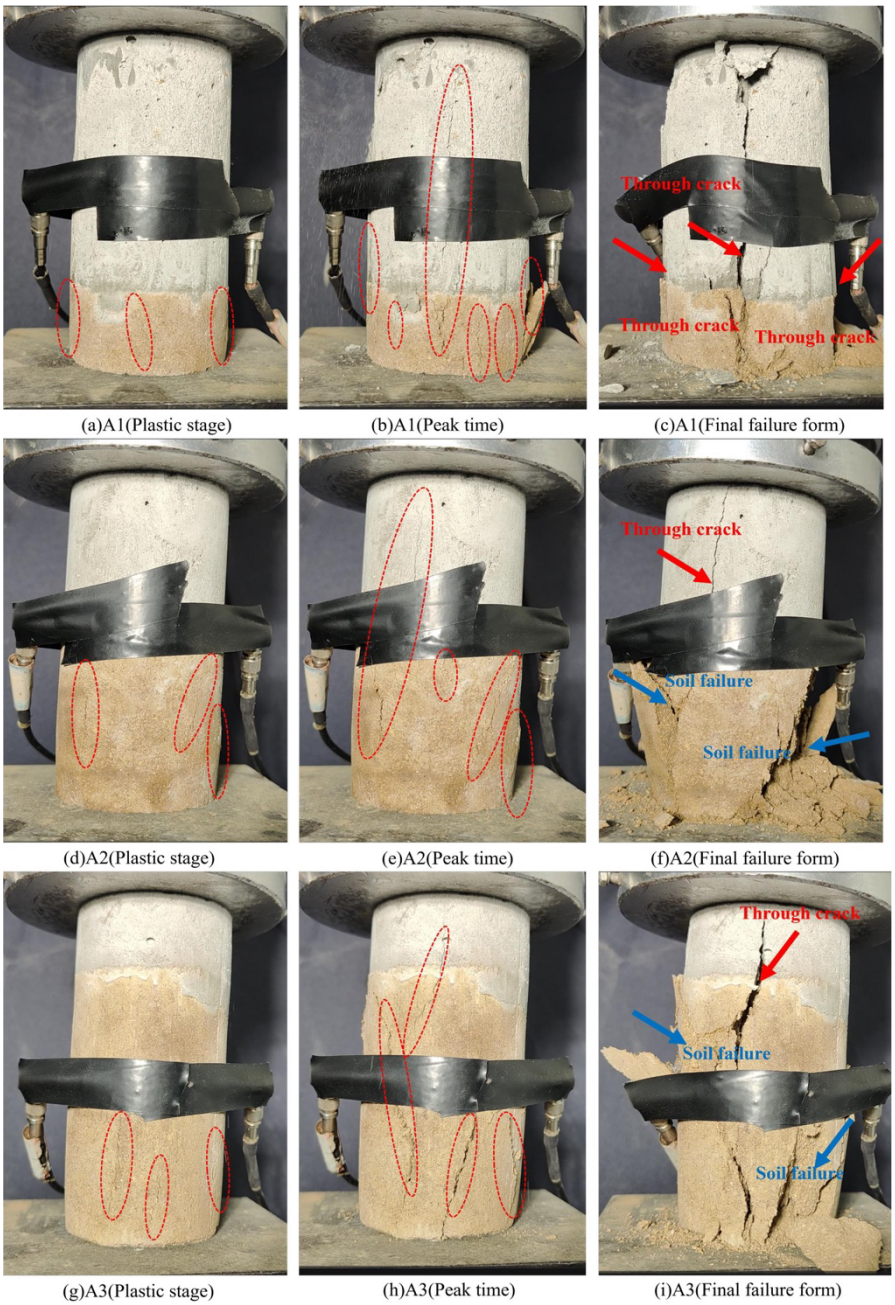


**Fig. 6.** Crack evolutions on surfaces of foam concrete–soil composites with different height ratios

A1 enters the plastic stage at about 66.7% of the peak stress. Fig. 6(a) shows a local swelling phenomenon in the central area of the soil layer. Subsequently, three vertical cracks are formed. When stress is loaded to the peak (2.972 MPa), Fig. 6(b) shows cracks in the soil layer propagating toward the upper and lower sides. Specifically, the upward crack propagation breaks the composite interface and extends to the foam concrete layer. The post-peak failure stage is short, and the bearing capacity falls suddenly and quickly to 90% of the peak stress after reaching the peak because local buckling occurs after fast crack propagation. In this stage, cracks proliferate, and microcracks connect and extend into through cracks. The deformation capacity after sample failure increases substantially, and the bearing capacity is 2.036 MPa, which is maintained at a high level because frictional forces are produced on two sides of the fracture surface. Hence, samples still have some bearing capacity.

Figs. 6 (d)–(i) show A2 and A3 have crack propagation characteristics similar to A1. Cracks begin from the center of the soil layer in the plastic stage (about 50%–60% of the peak stress). With the increase of loads, cracks spread gradually and connect and extend into through cracks. However, only one crack on the soil layer surfaces of A2 and A3 runs through the foam concrete–soil interface and spreads to the foam concrete layer, while the rest of the cracks only propagate in the soil layer. On the contrary, many cracks are in A1. Additionally, the bearing capacities of A2 and A3 after fracture failure are 0.567 and 0.278 MPa, respectively, which are much lower than that of A1 due to unique porous structures in foam concrete. Pores are closed upon compressive failure. Matrices in the rest of the shear zones develop friction and interlocking behaviors, thus

resulting in excellent deformation performances and buffer performances of foam concrete. Therefore, the post-failure bearing capacity of A1 with a thicker foam concrete layer is higher than those of A2 and A3.

### 4.2 Crack propagation characteristics of composites under vibration loads

For a deeper analysis of crack propagation evolutionary laws of foam concrete–soil composites with different height ratios under vibration loads, their cumulative acoustic emission hits are plotted in 3D space diagrams, as shown in Fig. 7. Moreover, the acoustic emission hits of composites under vibration loads are analyzed.

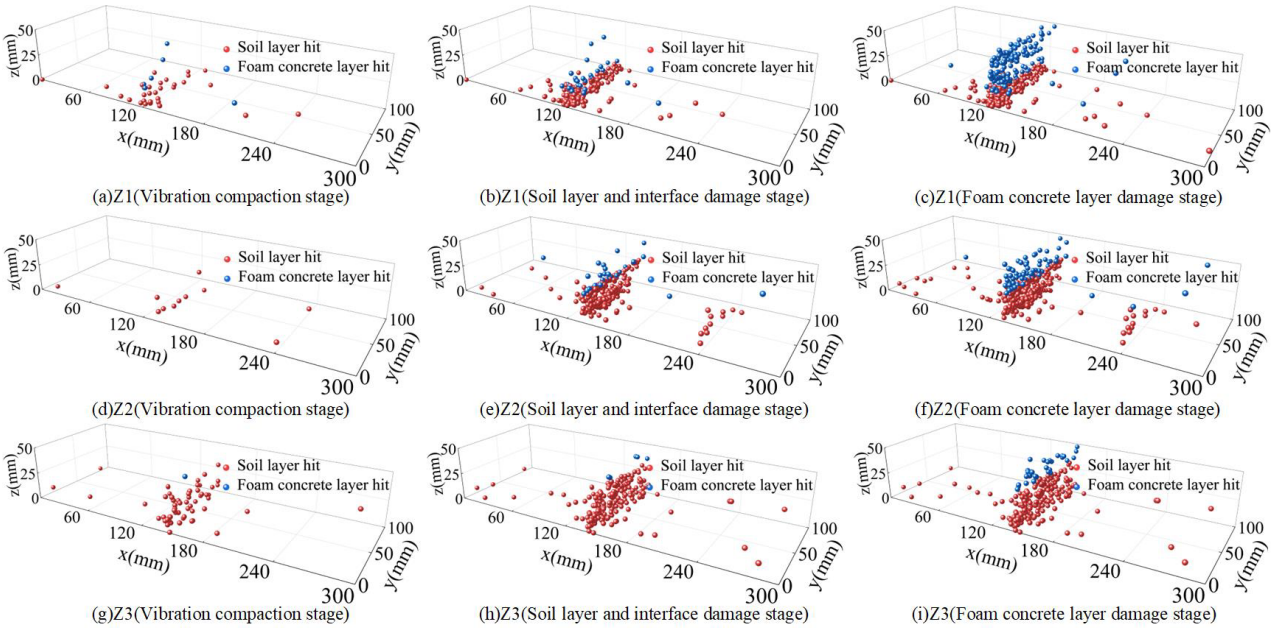


**Fig. 7.** Cumulative acoustic emission hits of foam concrete–soil composites with different height ratios

Fig. 7 shows damages initiate from the bottom soil layer in all three composites under vibration loads and then spread upward as the vibration continues. Finally, damages cross over the foam concrete–soil interface and enter the foam concrete. Taking Z1 for example, the acoustic emission hits of Z1 along the z direction mainly concentrate within 0–6 mm from 0 s to 184 s, accounting for 76.3%. In this stage, hits are primarily produced by vibration-induced closure of microcracks inside composites. From 184 s to 303 s, the acoustic emission hits along the z direction concentrate within 0–12.8 mm, accounting for 88.2%. Damages initiate from the bottom soil layer. Many acoustic emission hits are produced at the foam concrete–soil interface (12.5 mm) because foam concrete stops crack propagation temporarily, and damages accumulate in the foam concrete layer near the interface. With continuous vibration excitation, major damages of Z1 spread upward gradually. From 303 s to 385 s, the acoustic emission hits along the z direction concentrate within 14.7–50 mm, accounting for 91%. Damages of Z1 are focused on the foam concrete layer. From 385 s to 434 s, few hits are produced, accounting for only 9.6% of total hits in the whole process. This section is the residual bearing, and damages are mainly at the foam concrete layer. According to acoustic emission positioning laws, the damage stages of foam concrete–soil composite can be divided into the initial compaction section, soil layer and interface damage stage, foam concrete layer damage stage, and residual bearing stage.

The damage positioning results show the damages of Z1, Z2, and Z3 along the x direction concentrate within the ranges of 100–135, 120–150, and 130-160 mm, respectively. The crack propagation of composite skews slightly to the left with increased foam concrete thickness due to unique porous structures in foam concrete, and irregular foam cell bodies are connected under vibration excitation, generating some offsets.

### 4.3 Gaussian mixture model-based analysis of crack damage modes of composites under dynamic and static loading conditions

Tensile and shear cracks are major crack damage modes in the damage failure of materials. The AF-RA ratio can be used to distinguish tensile cracks and shear cracks [20]. However, AF-RA ratios often vary in different materials. Accurately determining the threshold of tensile and shear cracks according to the RA-AF diagram is difficult. The Gaussian mixture model is a clustering algorithm used to solve situations when data of the same set contains several different distributions. The mixture density of Gaussian mixture model is defined as follows [21]:

$$p(\vec{x} \mid \lambda) = \sum_{i=1}^{M} \omega_i N_i(\vec{x} \mid \vec{\mu}_i, \Sigma_i), i = 1, \cdots, M \tag{1}$$

where $M$ is the number of mixture models, and $M = 2$. $\omega_i$ is the mixture weight coefficient, and it meets $\sum_{i=1}^{M} \omega_i = 1$. $N_i(\vec{x} \mid \vec{\mu}_i, \Sigma_i)$ is the Gaussian probability density function of the single peak i.

In this study, a clustering analysis based on distribution characteristics of the RA-AF diagram is carried out through a 2D Gaussian mixture model, thus obtaining the percentage of cracks in foam concrete–soil composites in different stages under dynamic and static loading conditions. The results are shown in Fig. 8.

Figs. 8(a)–(c) show that the cracks in all stages of the three composites are dominated by shear cracks under uniaxial compression. A1, A2, and A3 all develop tensile-shear mixed failures dominated by shear failures. Moreover, the foam concrete–soil composites develop cracks quickly under compression loads in the plastic stage and post-peak failure stage. With the reduction of foam concrete thickness, shear cracks decrease from 99% to 76.7% in the plastic stage and from 88.3% to 52.3% in the post-peak failure stage. The plasticity of the composite is enhanced continuously while bending shearing cracks decrease gradually. Figs. 8(d)–(f) show that different from uniaxial compression, the failure modes of composites under vibration loads change. With the decrease of foam concrete thickness, the failure mode of composite shifts from the shear failure-dominated mode to the tensile fracture-dominated mode.

Proportions of shear cracks in A1, A2, and A3 under uniaxial compression failure are 92.7%, 83%, and 82.8%, respectively. Proportions of shear cracks of Z1, Z2, and Z3 throughout the vibration failure are 75.4%, 38.4%, and 19.1%, respectively. Both decrease with the decrease of the foam concrete proportion because with the reduction of the proportion of the foam concrete, the cell body strengths of composite samples decline. A composite sample with a higher proportion of foam concrete has stronger cohesion, and the shear resistance of matrix cohesion gradually becomes the major bearing capacity, resulting in more shear cracks in the failure. When the soil layer accounts for a high proportion, the composite sample has small cohesion and develops irregular lateral compression failures, thus developing abundant tensile cracks.

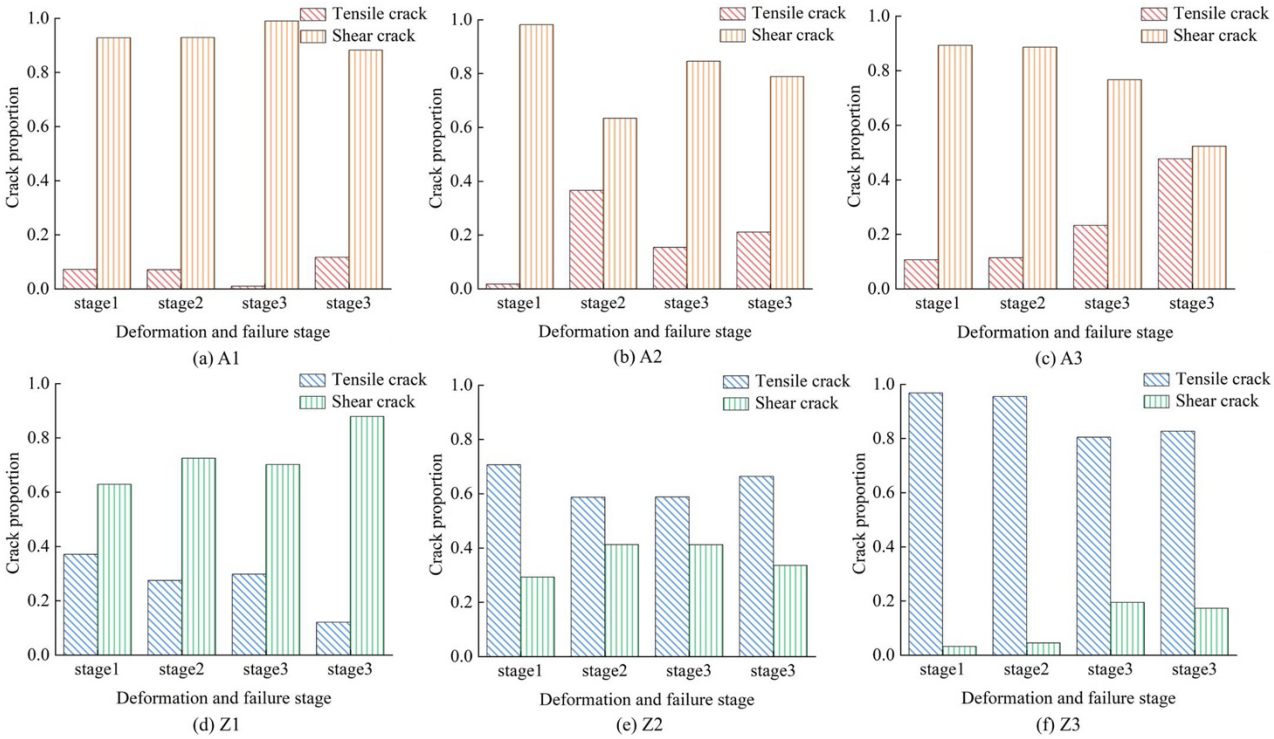


**Fig. 8.** Crack proportions of foam concrete–soil composites with different height ratios under dynamic and static loading conditions

### 4.4 Crack propagation scale analysis of composites under dynamic and static loading conditions

The b value is essential in the relationship between earthquake magnitude and frequency. The dynamic evolution laws of the crack propagation scale of materials can be analyzed through the b value. A high b value indicates weak damages, whereas a low b value indicates substantial damages [22]. The acoustic emission b value is calculated by the maximum likelihood estimation method [23] as follows:

$$b = \frac{20 \lg e}{\bar{A} - A_{\min}} \tag{2}$$

where $\bar{A}$ is the average amplitude, and $A_{\min}$ is the minimum amplitude (unit: dB).

The fitting results of the b value are compared with the acoustic emission energy. The variation curves of energy and the b value of composite samples with time under dynamic and static loading conditions are plotted, as shown in Fig. 9.

Figs. 9 (a)–(c) show the b values of all three composites generally present a descending trend from the late elastic stage to the post-peak failure stage. In this process, macrocrack propagation occupies the dominant role. The minimum b value and peak energy are produced in the post-peak damage stage, thus creating the macroscopic fracture surface. The minimum b values of A1, A2, and A3 are 1.9, 1.594, and 1.492, respectively, and their peak energies are 148844, 24666, and 13900 mV·ms, respectively. With the reduction of foam concrete thickness, the minimum b value increases gradually, and the peak energy at generation of the macroscopic fracture surface declines gradually. The same law is observed under vibration. The b values of the three composites present a descending trend from the late stage of the soil layer and interface damage stage to the generation of the macroscopic fracture surface in the foam concrete damage stage. The minimum b values of Z1, Z2, and Z3 are 0.3, 0.474, and 0.566, respectively, and the peak energies are 8521443, 3132265, and 2568227 mV·ms, respectively. The laws are the same with the uniaxial compression. However, the b value under the vibration loads is generally smaller than that in uniaxial compression, and the released energy is

larger, indicating that the failure degree of the composite is more intensive under dynamic loads.

The evolutionary features of the b value also vary substantially among three foam concrete–soil composites under dynamic and static loading conditions. Before the macroscopic fracture of the composite under uniaxial compression, the acoustic emission b values of the compaction stage and elastic stage fluctuate and become stable. The b values in the soil layer and interface damage stage before the macroscopic fracture under vibration loads differ considerably. Moreover, substantial b value growths are noted before the macroscopic fracture surface production, which increase by 31.5%, 42.7%, and 23% due to energy storage when microcracks are connected and propagate into large-scale cracks.

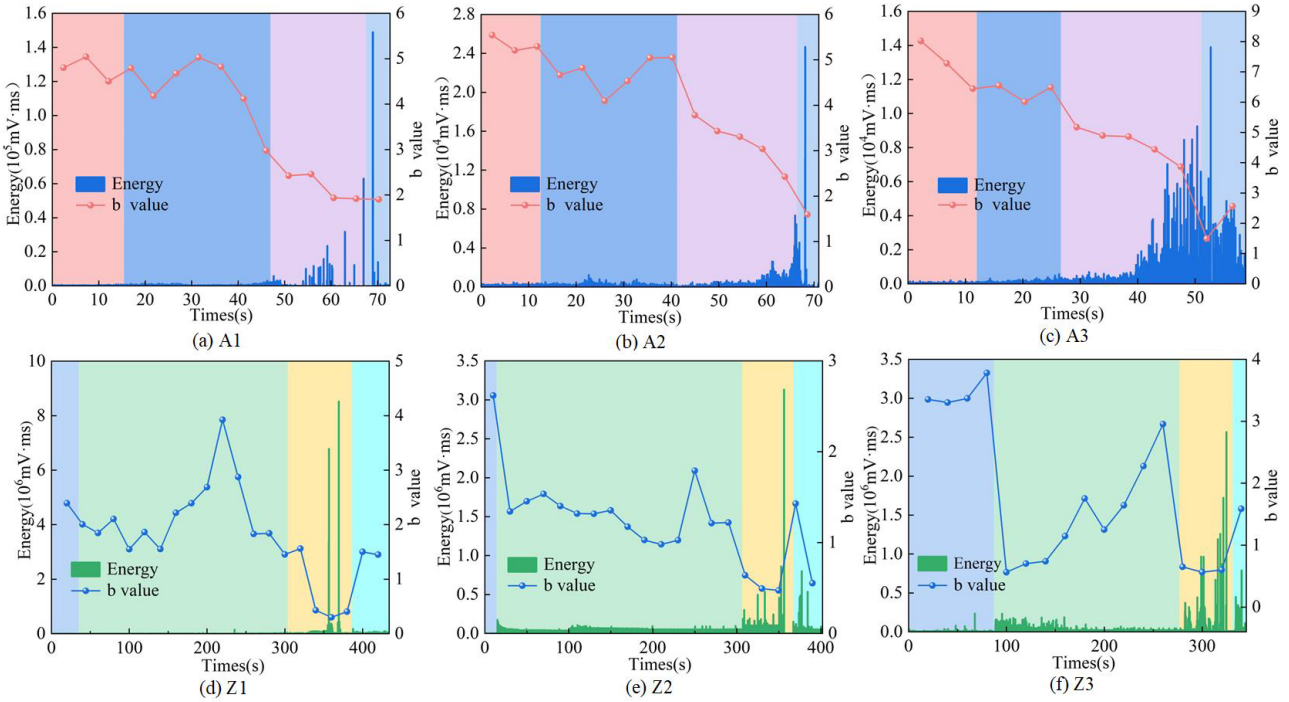


**Fig. 9.** Variation curves of energy and b value of foam concrete–soil composites with time under dynamic and static loading conditions

## 5. Conclusions

A uniaxial compression test and a vibration test of composite samples were carried out to study the crack propagation characteristics of foam concrete–soil composites with different height ratios under dynamic and static loading conditions. Moreover, damages in samples were monitored by acoustic emission. Critical attention was paid to analyzing the crack propagation, damage mode, and scale. The following conclusions could be drawn:

(1) Under uniaxial compression, all three foam concrete–soil composites with different height ratios begin to develop cracks in the middle of the soil layer at about 50%–70% of the peak stress. With the continuous stress loading, the cracks propagate toward the upper and lower sides and finally cross over the foam concrete–soil interface to form through cracks. Under vibration loads, the crack damages of all three composites concentrate within 100–160 mm along the x direction, and cracks initiate from the bottom soil layer. As vibration continues, cracks propagate upward, damages accumulate at the interface, and finally, the interface breaks to develop a macroscopic fracture.

(2) The proportions of shear cracks of foam concrete–soil composites with height ratios of 3:1, 1:1, and 1:3 under uniaxial compression loads are 92.7%, 83%, and 82.8%, respectively. All three composites develop the tensile-shear mixed failure dominated by shear failures. The proportions of shear cracks of foam concrete–soil composites with height ratios of 3:1, 1:1, and 1:3 under vibration loads are 75.4%, 38.4%, and 19.1%, respectively. With the reduction of foam concrete thickness, the failure mode shifts from the shear failure-dominated mode to the tensile fracture-dominated mode.

(3) The minimum b values of foam concrete–soil composites with height ratios of 3:1, 1:1, and 1:3 are 1.9, 1.594, and 1.492 under uniaxial compression load, respectively, and 0.3, 0.474, and 0.566 under vibration load, respectively. With the reduction of foam concrete thickness, the minimum b value under dynamic and static loading conditions increases gradually, and the released energy at the generation of the macroscopic fracture surface is low. Compared with uniaxial compression, the energy storage before macroscopic fracture under vibration loads is more prominent, manifested as the substantial increase of the b value before the macroscopic fracture.

In the vibration test of this study, the boundary conditions of foam concrete–soil composites are set on fixed supports on two sides. However, boundaries might need further optimization in the practical field due to the effects of dynamic and static loading in the traffic environment. Hence, the influences of boundary conditions closer to the field on the crack propagation of foam concrete–soil subgrade need to be studied further, which is conducive to improving the understanding of the mechanical properties of foam concrete backfilled subgrade.

**Acknowledgements**

The authors are grateful for the support provided by the Graduate Student Innovation Fund Project of Anhui University of Science and Technology (2022CX2035) and the Natural Science Foundation of China (52274070, 52204080).

## References

[1] H. M. Hamada, J. Y. Shi, F. Abed, A. M. Humada, and A Majdi, "Recycling solid waste to produce eco-friendly foamed concrete: A comprehensive review of approaches," *J. Environ. Chem. Eng.*, vol. 11, no. 6, Nov. 2023, Art. no. 111353.

[2] Y. Q. Qiu, Y. Liu, L. J. Zhang, and Z. Q. Wang, "Influence of Lightweight Foamed Concrete as Backfill Material on Stress and Deformation of Buttressed Earth-Retaining Wall," *Geofluids*, vol. 2021, pp. 1-14, Oct. 2021.

[3] T. Wang, Z. G. Ma, P. Gong, N. Li, and S. X. Cheng, "Analysis of Failure Characteristics and Strength Criterion of Coal-Rock Combined Body with Different Height Ratios," *Adv. Civ. Eng.*, vol. 2020, no. 11, Sep. 2020, Art. no. 8842206.

[4] S. Raj and K. Ramamurthy, "Physical, hydrolytic, and mechanical stability of alkali-activated fly ash-slag foam concrete," *Cem. Concr. Compos.*, vol. 142, Aug. 2023, Art. no. 105223.

[5] T. T. Nguyen *et al.*, "A micromechanical investigation for the effects of pore size and its distribution on geopolymer foam concrete under uniaxial compression," *Eng. Fract. Mech.*, vol. 209, no. 0, pp. 228-244, Mar. 2019.

[6] K. Wang, E. B. Zhao, Y. Y. Guo, F. Du, and L. Wang, "Deformation, seepage and energy evolution characteristics of gas-bearing coal-rock under intermediate principal stress," (in Chinese), *J. Min. Sci. Technol.*, vol. 8, no. 1, pp. 74-82, Feb. 2023.

[7] H. Yoshihara and M. Maruta, "Mode II critical stress intensity factor of solid wood obtained from the asymmetric four-point bend fracture test using groove-free and side-grooved samples," *Eng. Fract. Mech.*, vol. 258, no. 0, Nov. 2021, Art. no. 108043.

[8] A. Gani, J. M. Banday, and D. C. Rai, "Shake table tests on timber frame structure infilled with dry bond masonry," *J. Build. Eng.*, vol. 78, Sep. 2023, Art. no. 107597.

[9] Z. C. Huang *et al*, "Field assessment of a subgrade-culvert transition zone constructed with foamed concrete in the ballasted railway," *Int. J. Rail Transp.*, to be published. Accessed: Feb. 23, 2023. doi: 10.1080/23248378.2023.2181877. [Online]. Available: https://doi.org/10.1080/23248378.2023.2181877

[10] X. N. Shi, J. J. Huang, and Q. Su, "Experimental and numerical analyses of lightweight foamed concrete as filler for widening embankment," *Constr. Build. Mater.*, vol. 250, no. 0, Jun. 2020, Art. no. 118897.

[11] D. L. Yang *et al.*, "Study on Interface Bonding Properties between Foamed Ceramics and Foamed Concrete," *Sustainability*, vol. 14, no. 4094, Apr. 2022, Art. no. 4094.

[12] H. Y. Zhou *et al.*, "A novel energy-absorbing composite structure with layers of basalt fiber fabric constraining waste brick particles and foam concrete," *Constr. Build. Mater.*, vol. 387, Jun. 2023, Art. no. 131579.

[13] N. W. Portal, M. Flansbjer, K. Zandi, L. Wlasak, and K. Malaga, "Bending behaviour of novel Textile Reinforced Concrete-foamed concrete (TRC-FC) sandwich elements," *Compos. Struct.*, vol. 177, no. 0, pp. 104-118, Aug. 2017.

[14] E. A. Flores-Johnson, B. A. Company-Rodriguez, J. F. Koh-Dzul, and J. G. Carrillo, "Shaking Table Test of U-Shaped Walls Made of Fiber-Reinforced Foamed Concrete," *Materials*, vol. 13, no. 11, Aug. 2020, Art. no. 2534.

[15] N. 'A. A. Murad, N. A. Rahman, A. H. A. Firdaus1, and S. A. A. Khairuddin, "Strength of Modified Foam Concrete-Filled Hollow Section Using Fly Ash as Sand Replacement," in *IOP Conf. Ser.: Mater. Sci. Eng.*, 2021, vol. 1200, Art. no. 012016.

[16] V. Valaskova, J. Vlcek, and M. Drusa, "Experimental and computational dynamic analysis of the foam concrete as a sub-base layer of the pavement structure," in *MATEC Web Conf.*, 2018, vol. 211, Art. no. 13002.

[17] R. A. A. Lima, M. Drobiazko, A. Bernasconi, and M. Carboni, "On crack tip localisation in quasi-statically loaded, adhesively bonded double cantilever beam specimens by acoustic emission," *Theor. Appl. Fract. Mech.*, vol. 118, Jun. 2022, Art. no. 103286.

[18] Z. J. Wang, J. J. Zhang, K. M. Yan, J. B. Wu, and X. N. Deng, "Model soil design considering similitude of dynamic constitutive model and evaluation of similarity level," (in Chinese), *Rock Soil Mech.*, vol. 36, no. 5, pp. 1328-1332, May. 2015.

[19] J. H. Zou *et al.*, "Field vibration test and analysis of underground structure under vehicle loads," (in Chinese), *J. Build. Struct.*, vol. 43, no. 5, pp. 195-204, May. 2022.

[20] M. De Smedt, K. Andreev, N. Shetty, and E. Verstrynge, "Effectiveness of acoustic emission parameters to monitor the crack formation in refractories – Case study on castables of different brittleness," *J. Eur. Ceram. Soc.*, vol. 39, no. 16, pp. 5423-5432, Oct. 2019.

[21] D. A. Reynolds and R. C. Rose, "Robust text-independent speaker identification using Gaussian mixture speaker models," *IEEE Trans. Speech Audio Process.*, vol. 3, no. 1, pp. 72-83, Jan. 1995.

[22] P. R. Prem, M. Verma, and P. S. Ambily, "Damage characterization of reinforced concrete beams under different failure modes using acoustic emission," *Structures*, vol. 30, pp. 174-187, Apr. 2021.

[23] L. J. Dong and L. Y. Zhang,"Error analysis of b-value of acoustic emission for rock fracture," (in Chinese), *J. Yangtze River Sci. Res. Inst.*, vol. 37, no. 8, pp. 75-81, Aug. 2020.